DESIGN OF MICROSTRIP ARRAY ANTENNA BY USING ACTIVE ELEMENT PATTERN TECHNIQUE COMBINING WITH TAYLOR SYNTHESIS METHOD

Q.-Q. He and B.-Z. Wang

Institute of Applied Physics
University of Electronic Science and Technology of China
Chengdu 610054, China

Abstract—Active element pattern technique is applied for analyzing microstrip array, which divides a large array analysis problem as a superposition of various simplified small array problems and greatly reduces the computation burden. The effects of the mutual coupling and the surrounding array environment are rigorously taken into account in the proposed method. Based on the active element pattern technique, a low side lobe microstrip array is synthesized. The commercial full-wave simulation software, HFSS, is used to simulate the array as a whole and the efficiency of the proposed method is validated.

1. INTRODUCTION

Analysis and design of array antennas are complicated by the presence of mutual coupling in the array environment [1–7]. Direct analysis approaches for array antenna mounted on arbitrarily shaped platforms are typically based on either the method of moments (MoM) [8–12], finite element methods (FEM) [13], or finite difference time domain (FDTD) techniques [14, 15]. In [16], a uniform theory of diffraction combining with numerical algorithm is used to calculate the mutual coupling between circular apertures on a doubly curved surface. In [17–19], an efficient and accurate hybrid method based on the combination of the method of moments with a special Green's function is presented to analyze antenna and arrays. In [20], the effect of the mutual coupling between the array elements on the performance of the adaptive array antennas is investigated when the actual received voltages which include the mutual coupling are directly used to estimate the weight vector based on the adaptive algorithm. Furthermore, Zhao et al. [21]

use an efficiency-optimized scheme to design an optical phased array. Nie et al. [22] apply the integral equation combining with physical optics method to analyse the slot array enclosed in an electrically large radome. Unfortunately, these approaches are time-consuming, especially for arrays with complex elements or mounted on complex platforms.

Active element pattern technique [23, 24], which uses the measured or calculated patterns of individual elements in the array environment to calculate the pattern of the fully excited array, can often be employed when numerical techniques cannot. Of course, if it is possible to compute the active element patterns using a given technique, then the fully excited array can usually be analyzed using the same technique. However, active element pattern technique usually permits faster pattern calculations than other methods once the element pattern data are available. Therefore, active element pattern technique is often preferable to other techniques. Though the subject of mutual coupling is included in much of the array antenna literatures, array analysis method based on active element pattern is still few in recent years.

In this paper, we investigate microstrip arrays by using active element pattern technique and design a low side lobe microstrip array by applying the Taylor line source synthesis method. The effects of the mutual coupling and the surrounding array environment are rigorously taken into account in the proposed method. Compared with those numerical approaches mentioned above, the proposed method has the advantages of reduced computation burden and simplified implementation.
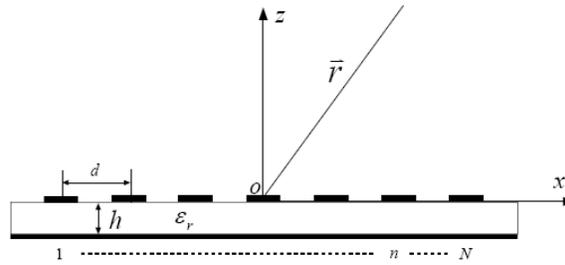

Figure 1. Geometry of a microstrip linear array of N elements.

2. FORMULATION

The active element pattern is defined as the radiation pattern of the array when one radiating element is driven and all others are terminated with matched loads. In order to illustrate the active element pattern technique, a microstrip linear array of N elements is used, as shown in Fig. 1. By the principle of superposition, the far field radiated by a fully excited array can be expressed using active element patterns as

$$\mathbf{E}_{total} = \sum_{n=1}^{N} I_n \mathbf{G}_a^n(\theta, \varphi) e^{jk\hat{\mathbf{r}} \cdot \mathbf{r}_n} \tag{1}$$

where I_n is the complex valued feed current applied to the nth element, $\mathbf{G}_a^n(\theta, \varphi)$ is the active element pattern of the nth element, $\exp(jk\hat{\mathbf{r}} \cdot \mathbf{r}_n)$ is the spatial phase term, $\hat{\mathbf{r}}$ is the unit radial vector from the coordinate origin in the observation direction (θ, φ), and $\mathbf{r}_n$ is a position vector from the origin to the center of the nth element; boldface type indicates a vector quantity.

In the expression of (1), the coordinate vector of the nth element can be given by

$$\mathbf{r}_n \cdot \hat{\mathbf{r}} = x_n \cos \varphi \sin \theta \tag{2}$$

$$x_n = \left(n - \frac{N+1}{2} \right) d, \quad n = 1, 2, 3, \ldots, N \tag{3}$$

where d is the distance between neighbor two elements.

Note that the sequence $\{\mathbf{G}_a^n(\theta, \varphi)\}$ contains all of the mutual coupling effects associated with the array environment and the excitation of the element. Furthermore, the sequence $\{\mathbf{G}_a^n(\theta, \varphi)\}$ also implies that the active element pattern depends on the position of the particular feed element in the array.

If the array is periodic and infinite, the active element patterns are identical for all elements in the array. If the array is large, the active element patterns can be seen as approximate identical for interior elements in the array. Therefore, the array elements can be divided into edge elements, interior elements, and adjacent edge elements, where the adjacent edge elements locate between edge elements and interior elements.

Thus, the far field of (1) can be divided into three parts as follows

$$\mathbf{E}_{total} = \mathbf{E}_e(\theta, \varphi) + \mathbf{E}_i(\theta, \varphi) + \mathbf{E}_{ae}(\theta, \varphi) \tag{4}$$

where $\mathbf{E}_e(\theta, \varphi)$ is the superposition of the active element patterns of all edge elements; $\mathbf{E}_i(\theta, \varphi)$ is the superposition of the active element

patterns of all interior elements; $\mathbf{E}_{ae}(\theta, \varphi)$ is the superposition of the active element patterns of all adjacent edge elements; and

$$\mathbf{E}_e(\theta, \varphi) = \sum_{s=1}^{N_e} I_s \mathbf{G}_a^s(\theta, \varphi) e^{jk\hat{\mathbf{r}} \cdot \mathbf{r}_s} \tag{5}$$

$$\mathbf{E}_i(\theta, \varphi) = \mathbf{G}_{av}(\theta, \varphi) \sum_{l=1}^{N_i} I_l e^{jk\hat{\mathbf{r}} \cdot \mathbf{r}_l} \tag{6}$$

$$\mathbf{E}_{ae}(\theta, \varphi) = \sum_{m=1}^{N_{ae}} I_m \mathbf{G}_{ae}^m(\theta, \varphi) e^{jk\hat{\mathbf{r}} \cdot \mathbf{r}_m} \tag{7}$$

where N_e is the number of all edge elements, N_i is the number of all interior elements, and N_{ae} is the number of all adjacent edge elements.

Compared with the expression of (1), the active element pattern of interior element in (6) only needs to be calculated once by using a small arraywhereas the active element patterns of interior elements in (1) need to be calculated element-by-element in the whole array. Thus, the computation burden is reduced remarkably.

For certain applications, the far field of (4) with low side lobe levels (SLLs) should be provided to avoid electromagnetic interference. In order to obtain low SLLs, the Taylor line source method is considered [25]. In the expression of (4), the required current distribution can be presented as follows

$$I(x_n) = \frac{\lambda}{Nd} \left[1 + 2 \sum_{p=1}^{\bar{n}-1} S(p, A, \bar{n}) \cos\left(2\pi p \frac{x_n}{Nd} \right) \right] \tag{8}$$

where the parameter $\bar{n}$ is a constant chosen by the designer and determines the number of pattern zeros that are modified from the $\sin x$ over x pattern. The coefficients $S(p, A, \bar{n})$ are the samples of Taylor line source pattern, and is given by

$$S(p, A, \bar{n}) = \frac{[(\bar{n}-1)!]^2}{(\bar{n}-1+p)!(\bar{n}-1-p)!} \prod_{k=1}^{\bar{n}-1} \left[1 - \left(\frac{p}{\sigma\sqrt{A^2+(k-1/2)^2}} \right)^2 \right],$$
$$|p| < \bar{n} \tag{9}$$

where the parameter A is related to the maximum desired side lobe level R_0 by

$$A = \frac{1}{\pi} \cosh^{-1}(R_0) \tag{10}$$

The scaling factor σ is determined by making the zero location, and it is given by

$$\sigma = \frac{\bar{n}}{\sqrt{A^2 + (\bar{n} - 1/2)^2}} \tag{11}$$

3. ANALYSIS AND DESIGN OF A MICROSTRIP ARRAY

3.1. Laboratory Model

A microstrip linear array is used to test the active element pattern technique given above. The radiating elements are mounted on the surface of the dielectric substrate with a thickness of $h = 0.762\,\text{mm}$ and a relative permittivity of $\varepsilon_r = 3$. Each radiating element is uniformly spaced from its neighbors by distances of $d = 0.51\lambda_0$ in the x-direction, where λ_0 is the free space wavelength corresponding to an operating frequency of $1.53\,\text{GHz}$.

A simple rectangle patch is selected as the radiating element, as shown in Fig. 2. In this design, the operating frequency is mainly determined from the rectangular patch dimensions and the feed position. According to [26], the length L of the rectangular patch is chosen to be $60.6\,\text{mm}$ and the width W of the rectangular patch is chosen to be $55.5\,\text{mm}$. By moving the feed position along the x-axis, a resonant frequency can be obtained at feed position B. By moving the feed position along the y-axis, the other resonant frequency can be obtained at feed position A. Calculated and measured resonant frequencies are shown in Table 1. It is clear that a good agreement is obtained between calculated and measured results.
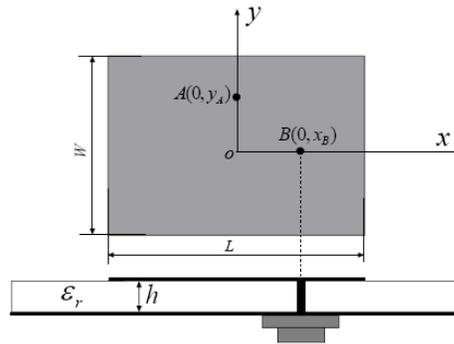

Figure 2. Geometry of an array element for different feed positions.

Table 1. The calculated and measured results.

Position (mm)	Means	Resonant Frequency	Source of Data
Feed Point A (0, 9.5)	Calculated	1.53 GHz	HFSS
	Measured	1.54 GHz	Reference [26]
Feed Point B (9.6, 0)	Calculated	1.41 GHz	HFSS
	Measured	1.42 GHz	Reference [26]

3.2. Analysis and Extraction of Active Element Patterns

The crucial problem of the active element pattern technique comes from the computation of the active element patterns, where different types of the active element patterns are extracted, based on the particular position of the feed element in the array. Fig. 3 gives the calculated active element patterns of the left edge element, where different numbers of array elements are used. It is obvious that the active element pattern of 4-element array is in agreement with that of 3-element array completely. Thus, the mutual coupling to the left edge element comes mainly from its neighbor right-side two elements. The active element pattern of the left edge element can be obtained by using a 1×3 small array.

(a) xoz-plane   (b) yoz-plane
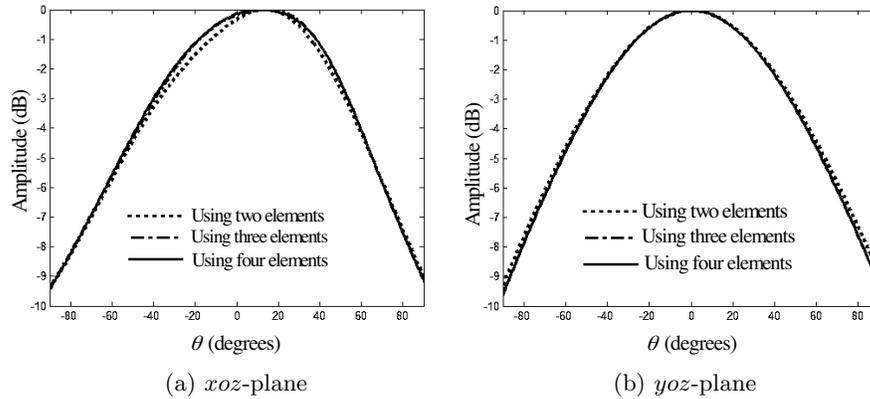
Figure 3. Calculated active element patterns for left edge element.

Similarly, the mutual coupling to the right edge element comes mainly from its neighbor left-side two elements. Note that the radiating

direction of the left edge element is different from that of the right edge element because of the different location of the excited element in the array. Thus, the active element pattern of the right edge element needs to be extracted by using a 1×3 small array different from its left edge counterpart.

As for interior elements, in order to obtain the active element pattern accurately, we compute the small array of 3-element, 5-element, and 7-element, respectively. Obviously, the active element pattern of 5-element array is in agreement with that of 7-element array, as shown in Fig. 4. Thus, the active element pattern of interior element can be extracted by using a 1×5 small array.

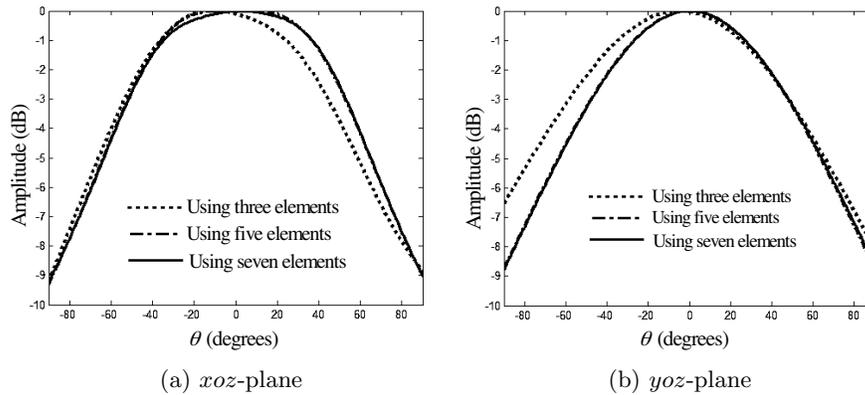

(a) *xoz*-plane   (b) *yoz*-plane

Figure 4. Calculated active element patterns for interior element.

Apparently, the array has adjacent edge elements, as shown in Fig. 5. Fig. 6 gives the active element patterns for the 3-element, 4-element, and 5-element arrays, respectively. It is clear that the active element pattern of 4-element array is in agreement with that of 5-element array. Therefore, the active element pattern of left adjacent edge element can be extracted by using a 1×4 small array. The active element pattern of right adjacent element can be obtained similarly.

3.3. Results and Discussions

Based on the analysis to active element pattern mentioned above, the active element patterns of edge elements, adjacent edge elements, and interior elements can be extracted by computing the 1×3, 1×4, and 1×5 small arrays, respectively.

Figure 7 presents the far field patterns for a 1×7 microstrip array by using active element pattern technique, HFSS simulation, and
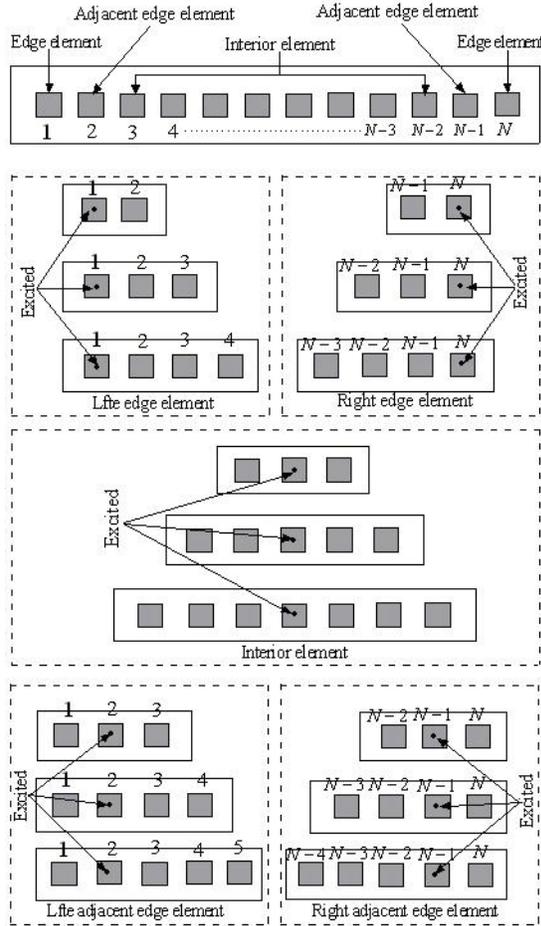
Figure 5. Flowchart of validating mutual effects for interior, edge, and adjacent edge elements, respectively.

classical array analysis method, respectively. From Fig. 7, we can see that the results of using active element pattern technique are consistent with that of using HFSS simulation when the 1×7 microstrip array is fully excited. Compared with classical array analysis method, the SLL is enhanced by 0.93 dB.

A 1×12 microstrip array is also synthesized by using the active element pattern technique combining with the Taylor line source synthesis method. Fig. 8(a) shows the normalized excitation currents based on a 30 dB Taylor weights. Fig. 8(b) gives the synthesis radiating
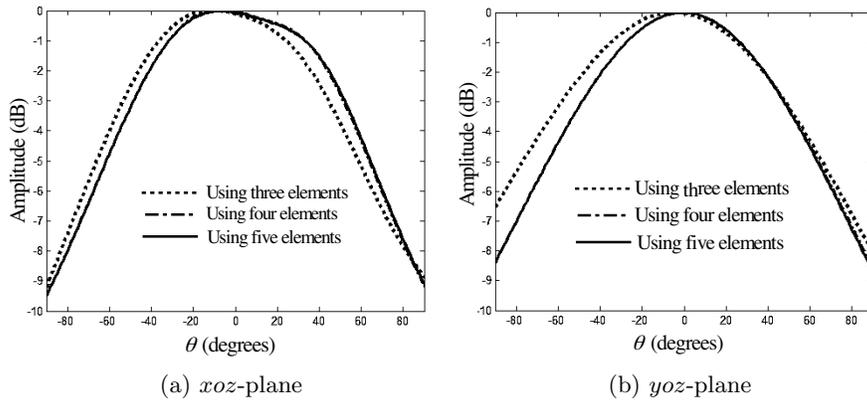
(a) xoz-plane

(b) yoz-plane

Figure 6. Calculated active element patterns for left adjacent element.
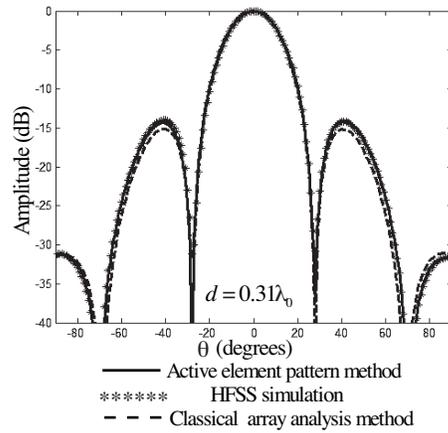

Figure 7. Far field patterns for 1×7 microstrip array in xoz-plane.

patterns. It is clear that active element pattern technique gives a bigger SLL value than that given by the classical array analysis method. The SLL is enhanced by 1.58 dB when the effects of the mutual coupling and the surrounding array environment are rigorously taken into account.

Fig. 9 shows the far field patterns for different values of the number of elements N. It is clear that, with the value of the number of elements N increasing, the results by using active element pattern technique are agreement with that by using classical array analysis method near the main radiation direction. Away from the main radiation direction, the coupling between elements became larger, and the results given by the two methods are different because classical array analysis method
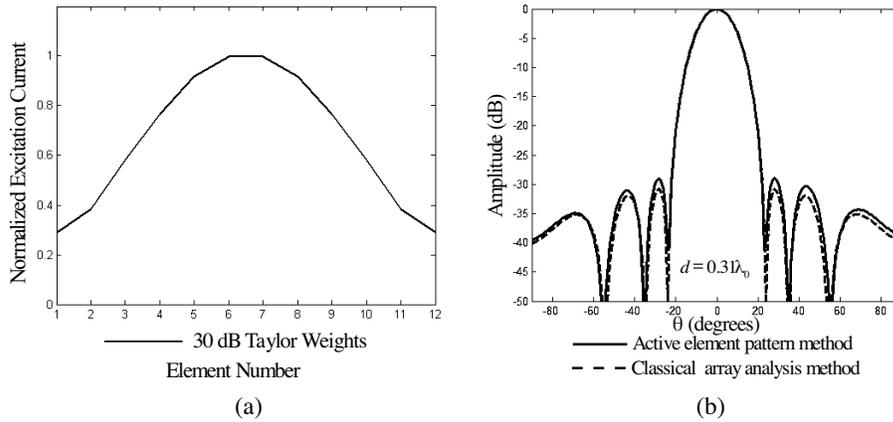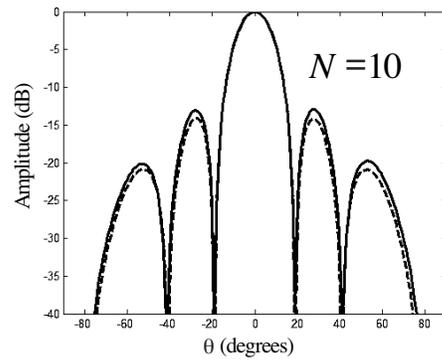
Figure 8. 30 dB Taylor weights and synthetic far field patterns for 1×12 microstrip array.

does not take into account the effects of the mutual coupling and the surrounding array environment.
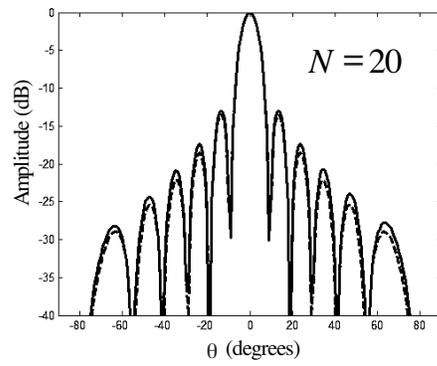
The CPU times by using different approaches are given in Table 2. In this calculation, the computer with an Intel P4 3.0-GHz processor and 4-GHz RAM is used. It is obvious that the active element pattern technique (AEPT) can effectively reduce the computation burden. We can also see that the computation burden can be reduced further when the number of the array elements is increased. When the number of

Table 2. Time cost comparison between the active element pattern technique (AEPT) and HFSS simulation.
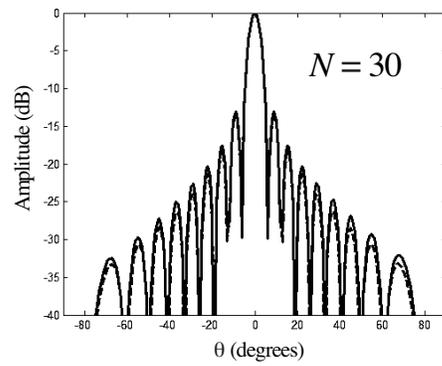
Element numbers of the array	7		12		Over 12	
Approach	AEPT	HFSS	AEPT	HFSS	AEPT	HFSS
Calculated time for edge elements	1327s	------	1327s	------	Effective	Incapable
Calculated time for adjacent edge elements	1505s	------	1505s	------		
Calculated time for interior elements	783s	------	783s	------		
Calculated time for the array	0.234s	16921s	0.265s	24485s		
Total time	3615.234s	16921s	3615.265s	24485s		

Figure 9. The far field patterns for different values of the number of elements N.

array elements is over 12, HFSS become incapable due to computer hardware limitation, but the active element pattern technique is still effective.

4. CONCLUSIONS

Active element pattern technique, in which the effects of the mutual coupling and the surrounding array environment are rigorously taken into account, combining with Taylor line source synthesis method is proposed and investigated. The proposed technique is effective when conventional array analysis methods are no longer adequate for arrays comprised of complex elements.

ACKNOWLEDGMENT

REFERENCES

1. Liu, H.-X., H.-Q. Zhai, L. Li, and C.-H. Liang, "A progressive numerical method combined with MOM for a fast analysis of large waveguide slot antenna array," *Journal of Electromagnetic Waves and Applications*, Vol. 20, No. 2, 183–192, 2006.

2. Zhang, Y. F. and W. Cao, "Array pattern synthesis based on weighted biorthogonal modes," *Journal of Electromagnetic Waves and Applications*, Vol. 20, No. 10, 1367–1376, 2006.

3. Krusevac, S., P. B. Rapajic, and R. Kennedy, "Mutual coupling effect on thermal noise in multi-element antenna systems," *Progress In Electromagnetics Research*, PIER 59, 325–333, 2006.

4. Fallahi, R. and M. Roshandel, "Effect of mutual coupling and configuration of concentric circular array antenna on the signal-to-interference performance in CDMA systems," *Progress In Electromagnetics Research*, PIER 76, 427–447, 2007.

5. Fu, Y. Q., Q. R. Zheng, Q. Gao, and G. H. Zhang, "Mutual coupling reduction between large antenna array using electromagnetic bandgap (EBG) structures," *Journal of Electromagnetic Waves and Applications*, Vol. 20, No. 6, 819–825, 2006.

6. Farkasvolgyi, A. and L. Nagy, "Mutual coupling effects on the mean capacity of MIMO antenna systems," *Progress In*

Electromagnetics Resarch Symposium 2007, 130–106, Prague, Czech Republic, Augst 27–28, 2007.

7. Jarchi, S., J. Rashed-Mohassel, and M. H. Neshati, "Mutual coupling of rectangular DRA in four element circular array," *Progress In Electromagnetics Resarch Symposium 2007*, 2000–2004, Beijing, China, March 26–30, 2007.

8. Yuan, T., L.-W. Li, M.-S. Leong, J.-Y. Li, and N. Yuan, "Efficient analysis and design of finite phased array of printed dipoles using fast algorithm: some case studies," *Journal of Electromagnetic Waves and Applications*, Vol. 21, No. 6, 737–754, 2007.

9. Liu, H.-X., H.-Q. Zhai, L. Li, and C.-H. Liang, "A progressive numerical method combined with MoM for a fast analysis of large waveguied slot antenna array," *Journal of Electromagnetic Waves and Applications*, Vol. 20, No. 2, 737–754, 2006.

10. Guo, J.-L., J.-Y. Li, and Q.-Z. Liu, "Analysis of antenna array with arbitrarily shaped radomes using fast algorithm based on vsie," *Journal of Electromagnetic Waves and Applications*, Vol. 20, No. 10, 1399–1410, 2006.

11. Papakanellos, P. J., "Alternative sub-domain moment methods for analyzing thin-wire circular loops," *Progress In Electromagnetics Resarch*, PIER 71, 1–18, 2007.

12. Matsushima, A., Y. Momoka, M. Ohtsu, and Y. Okuno, "Efficent numerical approch to electromagnetic scattering from three-dimensional periodic array of dielectric spheres using sequential accumulation," *Progress In Electromagnetics Resarch*, PIER 69, 305–322, 2007.

13. Qiu, Z. J., X. Y. Hou, X. Li, and J. D. Xu, "On the condition number of matrices from various hyberid vector FEM-BEM for mulations for 3-D Scattering," *Journal of Electromagnetic Waves and Applications*, Vol. 20, No. 13, 1797–1806, 2006.

14. Uduwawala, D., M. Norgren, P. Fuks, and A. Gunawardena, "A complete FDTD simulation of a real gpr antenna system operating above lossy and dispersive grounds," *Progress In Electromagnetics Resarch*, PIER 50, 209–229, 2005.

15. Losito, O., "Design of conformal tapered leaky wave antenna," *PIER Online*, Vol. 3, No. 8, 1316–1320, 2007.

16. Persson, P., L. Josefsson, and M. Lanne, "Investigation of the mutual coupling between apertures on doubly curved convex surface: Theory and measurements," *IEEE Transctions on Antennas and Propagation*, Vol. 51, No. 4, 682–692, Apr. 2003.

17. Ertürk, V. B. and R. G. Rojas, "Efficient analysis of input

impedance and mutual coupling of microstrip antennas mounted on large coated cylinders," *IEEE Transctions on Antennas and Propagation*, Vol. 51, No. 4, 739–748, Apr. 2003.

18. Ertürk, V. B., R. G. Rojas, and K. W. Lee, "Analysis of finite arrays of axially directed printed dipoles on electrically large circular cylinders," *IEEE Transctions on Antennas and Propagation*, Vol. 52, No. 10, 2586–2595, Oct. 2004.

19. Raffaelli, S., Z. Sipus, and P.-S. Kildal, "Analysis and measurements of conformal patch array antennas on multilayer circular cylinder," *IEEE Transctions on Antennas and Propagation*, Vol. 53, No. 3, 1105–1113, Mar. 2005.

20. Yuan, Q., Q. Chen, and K. Sawaya, "Performance of adaptive array antenna with arbitrary geometry in the presence of mutual coupling," *IEEE Transctions on Antennas and Propagation*, Vol. 54, No. 7, 1991–1996, July 2006.

21. Zhao, Y., X. Yang, Q. Cai, and W. Hu, "An optimized scheme for optical phased array beam steering controlled by wavelength," *PIER Online*, Vol. 3, No. 2, 127–131, 2007.

22. Nie, X.-C., Y.-B. Gain, N. Yuan, C.-F. Wang, and L.-W. Li, "An efficent hybrid method for analysis of slot arrays enclosed by large radome," *Journal of Electromagnetic Waves and Applications*, Vol. 20, No. 2, 249–264, 2006.

23. Guo, J.-L., J.-Y. Li, and Q.-Z. Liu, "Analysis of antenna array with arbitrarily shaped radomes using fast algorithm based on VSIE," *Journal of Electromagnetic Waves and Applications*, Vol. 20, No. 10, 1399–1410, 2006.

24. Pozar, D. M., "The active element pattern," *IEEE Transctions on Antennas and Propagation*, Vol. 42, No. 8, 1176–1178, Aug. 1994.

25. Taylor, T. T., "Design of line-source antennas for narrow beamwidth and low sidelobes," *IRE Transctions on Antennas and Propagation*, Vol. AP-3, 16–28, Jan. 1955.

26. Toh, B. Y., V. F. Fusco, and N. B. Buchanan, "Retrodirective array tracking prediction using active element characterisation," *Electronics Letters*, Vol. 37, No. 12, 727–728, Jun. 2002.

27. Ludwig, A. C., "Low sidelobe aperture distributions for blocked and unblocked circular apertures," *IEEE Transctions on Antennas and Propagation*, Vol. 30, No. 5, 933–946, Sept. 1982.

28. Chen, J. S. and K. L. Wong, "A single-layer dual-frequency rectangular microstrip patch antenna using a single probe feed," *Microwave and Optical Technology Letters*, Vol. 11, No. 2, 83–84, Feb. 1996.